# Solvent Effects on the Local Structure of *p*-Nitroaniline in Supercritical Water and Supercritical Alcohols

**Tomotsumi Fujisawa,*,† Masahide Terazima,† and Yoshifumi Kimura*,‡**

*Department of Chemistry, Graduate School of Science, Kyoto University, Kyoto, 606-8502, Japan, and Division of Research Initiatives, International Innovation Center, Kyoto University, Kyoto, 606-8501, Japan*

*Received: November 1, 2007; Revised Manuscript Received: March 21, 2008*

Raman spectra of *p*-nitroaniline in supercritical water and supercritical alcohols were measured, and the effects of solvents on the $NO_2$ and $NH_2$ stretching modes were investigated. The intensity and frequency of the $NO_2$ stretching mode significantly changed as a function of the solvent density and temperature. The frequency of the $NO_2$ stretching mode correlated with the absorption peak energy of the $S_1 \leftarrow S_0$ transition. On the other hand, the vibrational frequency of the $NH_2$ stretching mode did not correlate with the absorption peak shift, although it had a large frequency shift as a function of the density. The correlation between the $NO_2$ frequency and absorption peak energy suggested that the solvent effects of supercritical water and supercritical alcohols were similar to those for nonpolar solvents. The density functional calculation using the polarizable continuum model and *p*-nitroaniline−water clusters qualitatively reproduced the density dependence of the $NO_2$ stretching mode as well as the solvent polarity dependence. Detailed vibrational analysis revealed that the coupling between the $NO_2$ and C-$NH_2$ vibrational motions at the harmonic level has an important effect on the intensity and frequency shift of the $NO_2$ stretching mode. The frequency shift of the $NH_2$ stretching mode correlated with the degree of hydrogen bonding between the solvent molecules estimated from NMR measurements [Hoffmann M. M.; Conradi, M. S. *J. Phys. Chem. B.* **1998**, *102*, 263]. The existence of intermolecular hydrogen bonding around the $NH_2$ group was demonstrated even at low-density conditions.

## 1. Introduction

Supercritical fluid (SCF) technology has now spread over a variety of fields, including cleaning, synthesis, extractions, and separations. Among SCFs, supercritical water (SCW; $T_c = 647$ K) and supercritical alcohols (scAlcohols; $T_c = \sim 523$ K) have attracted much attention as environmentally benign solvents with unique properties for chemical applications.[1–5] Their characteristic features are wide tunabilities of dielectric constant and hydrogen bonding ability by changing temperature and pressure. To understand chemical processes occurring in these media, knowledge of intermolecular interactions such as solute−solvent hydrogen bonding is quite important.

Thus far, structures of SCW and scAlcohols have been investigated by various spectroscopic methods, including NMR, X-ray, and Raman spectroscopy.[5,7–11] Detailed information on the hydrogen bonding in SCW and scAlcohols has now been obtained, and the existence of hydrogen bonding has been demonstrated under supercritical conditions, except in the extremely gas-like region.[6–11] Measurements of reorientational relaxation and vibrational energy relaxation of the solvent molecules have clarified how hydrogen bonding influences these dynamics in the supercritical phase.[12,13]

On the other hand, studies on the solvation and solute−solvent hydrogen bonding in SCW and scAlcohols are still limited. Most studies to date have used absorption or fluorescence measurements of solvatochromic probe molecules to examine the local environment of the solute.[14–18] The main discussion has concentrated on the clustering of solvent molecules around the solute in the supercritical phase, the so-called "local density enhancement", which is a unique phenomenon occurring close to the critical point as a result of the solute−solvent attractive interaction and enhanced inhomogeneity in SCFs.[19,20] The dielectric continuum model has been a useful model to estimate the local density enhancement qualitatively. However, it is difficult to discuss solute−solvent hydrogen bonding using this model, because the model is based on only macroscopic parameters of solvents such as the dielectric constant and refractive index.

To estimate the strength of the solute−solvent hydrogen bonding in SCW and scAlcohols from the absorption measurements, the solvatochromic comparison method has been used so far.[21,22] On the basis of the solvatochromic comparison method, the solvatochromic parameters, $\alpha$ and $\beta$ values, were developed for the estimation of the degree of solute−solvent hydrogen bonding. The $\alpha$ value is a measure for the hydrogen bonding *donor* ability of solvents, which is determined by the difference in absorption maxima for *p*-nitroanisole and betaine dye 36, and the $\beta$ value is a measure for the hydrogen bonding *acceptor* ability of solvents determined by the difference in absorption maxima for *p*-nitroaniline (pNA) and *N*,*N*-diethyl-*p*-nitroaniline.[21] Lu et al. determined several solvatochromic parameters including $\alpha$ and $\beta$ values in supercritical ethanol (scEtOH) to examine polarity and hydrogen bonding.[15] They found the value of $\beta$ was almost equal to zero in the supercritical phase, while the value of $\alpha$ was around 0.5. Oka et al. measured absorption spectra of three well-known nitrobenzene derivatives (pNA, *N*,*N*-diethyl-*p*-nitroaniline, *p*-nitroanisole) in SCW.[23] They focused on the local density enhancement around pNA, and also examined solute−solvent hydrogen bonding by the evaluation of the $\beta$ value. Although they found that local density

* Corresponding author. TEL: +81-75-753-4024. FAX: +81-75-753-4000. E-mail address: fujisawa@kuchem.kyoto-u.ac.jp (T.F.); ykimura@kuchem.kyoto-u.ac.jp (Y.K.).
† Graduate School of Science.
‡ International Innovation Center.

10.1021/jp710530m CCC: $40.75 
Published on Web 05/16/2008

**SCHEME 1: Resonance Structures of pNA: (A) Neutral State; (B) Charge-Separated State**

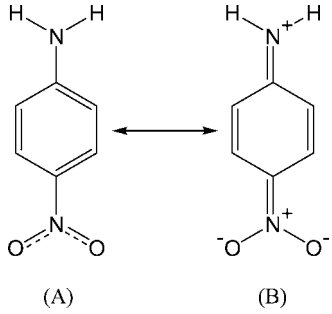


enhancement occurred under conditions fairly close to the critical point, they came to the conclusion that solute−solvent hydrogen bonding was negligible in SCW because the value of $\beta$ was equal to zero in the wide density range under supercritical conditions.

In the present work, we tried to evaluate the strength of solute−solvent interaction, especially with regard to the strength of solute−solvent hydrogen-bonding, in SCW and scAlcohols by directly measuring the specific vibrational modes of the solute molecules that are affected by solute−solvent hydrogen bonding. We have chosen pNA as the probe molecule. pNA is one of the well-known solvatochromic probes with a typical "push−pull" form, in which an electron-donating group and an electron-accepting group are connected by a conjugated $\pi$-system. As shown in Scheme 1, the electronic state is formally described by the resonance between a neutral state (A) and a charge-separated state (B). State A is dominant in the ground-state, and state B is dominant in the excited state. Experimental and theoretical investigations have been done for the electronic state as well as the vibrational state.[24,25] pNA has also attracted the interest of many spectroscopists with a main focus on the vibrational spectrum. The attention has been focused on the two strong $NO_2$ stretching modes for which the relative intensities have remarkable solvent polarity dependence.[26−30] In a previous report, we applied resonance Raman spectroscopy to investigate the solvation of pNA in SCW over a wide density range,[31] and found a remarkable change in the relative intensities and frequencies of the two $NO_2$ stretching bands as a function of pressure and temperature. The spectral change was discussed on the basis of the calculations of the electronic states of small pNA−water clusters with different compositions. In this research, we performed more detailed studies on the vibrational spectra of pNA in scAlcohols together with SCW, extending the measurements to the $NH_2$ stretching region (3000−3500 $cm^{-1}$). The $NH_2$ stretching mode is a direct probe for intermolecular hydrogen bonding with surrounding solvents. Here, we discuss solute−solvent hydrogen bonding and its effects on the molecular structure of pNA in SCW and scAlcohols. The results indicate that the estimation of solute−solvent interaction using a solvatochromic parameter, such as the $\beta$ value, is insufficient for SCW and scAlcohols.

## 2. Experiment

**2.1. Apparatus.** Raman spectra were measured with a back scattering geometry using a charge-coupled device (CCD) camera with Peltier cooling (Princeton Instruments; Spec-10: 400BRXTE) attached to a 64 cm monochromator (Jobin Yvon, T64000) with 1800 and 600 lines $mm^{-1}$ gratings. The fingerprint region was measured under the resonant condition using the 363.8 nm line of an Ar ion laser (Coherent, Enterprize) or the third harmonic output from a pulsed Nd:YAG laser (Continuum, Minilite) operated at 15 Hz for excitation. Since the $NH_2$ stretching mode was not observed under the resonant condition, the mode was measured for the nonresonant condition using the 514.5 nm line of the Ar ion laser. An appropriate edge filter (Semrock) was placed in front of the slit of the monochromator to remove stray light. To obtain a good signal-to-noise ratio, the Raman spectrum was accumulated for 0.5−1 h. A detailed description of the high-pressure and high-temperature system has been described elsewhere.[32] Briefly, a high-pressure cell, which was made of corrosive-resistant Hastelloy C, was equipped with two sapphire windows (3.5 mm diameter, 2 mm thickness). An alternative cell, which was made of SUS630, was also usable at our experimental conditions. The aperture angle of the window was made 45° to collect the scattering from the sample effectively, and the optical path length was approximately 5 mm. The sample solution, which was continuously bubbled by dry nitrogen or argon before pumping, was flowed into the high-pressure cell at a rate of 1.0−1.5 mL/min using an high-performance liquid chromatography (HPLC) pump (Jasco, PU-2080plus) in a single-pass configuration. Without bubbling, pNA decomposed at supercritical temperatures probably because of a reaction with dissolved oxygen, and the Raman spectrum was not observed because of the significant overlap with impurity fluorescence. With bubbling, sample degradation was sufficiently suppressed, which was confirmed by the absorption spectrum of the sample solution having passed through the optical cell after the high-temperature experiment. The pressure of the system was controlled by a back pressure regulator (Jasco, 880−81) with an accuracy of about ± 0.3 MPa. The temperature of the cell was regulated within an accuracy of ±1 K by a sheathed heater wound around the cell and a thermocouple directly inserted into the sample chamber. Typically, 3 h were required to raise and stabilize the temperature of the cell from room temperature to the supercritical temperature. For measuring the Raman spectrum in vapor, the sample was enclosed in a quartz cell that was evacuated by a vacuum pump to ∼4 Pa. The cell was then placed in a brass jacket, which was heated by a sheathed heater.

The absorption spectra under high-pressure and high-temperature conditions were measured using the same cell described above. A $D_2$ lamp (Otsuka Electronics, MC-964) was used as a light source, and a multichannel photo detector (Otsuka Electronics, MCPD-1000) was used as a detection system.

**2.2. Materials.** Ethanol (EtOH, spectra grade), methanol (MeOH, spectra grade), reference solvents (acetonitrile, tetrahydrofuran, benzene, and cyclohexane (spectra grade)), and pNA were purchased from Nacalai Tesque. Deuterated ethanol ($C_2H_5OD$, >99.5% D) was purchased from Aldrich. All solvents were used as received, and pNA was recrystalized from ethanol before use. Ion-exchanged water produced by a Milli-Q system (>18 Ω $cm^{-1}$) was used. The concentration of the sample solution was prepared to be about 1−5 mM and 50 mM for resonance and nonresonance Raman measurements, respectively. Raman spectra were recorded under the following conditions. In water, the isobar and isotherm were 30.4 MPa and 668.5 K, respectively; in MeOH, 40.2 MPa and 541 K, respectively; and in EtOH, 30.9 MPa and 538 K, respectively. The densities of water, methanol, and ethanol are taken from ref 33.

**2.3. Computational Method.** The ground-state geometry optimization and normal-mode analysis of pNA were performed by density functional theory (DFT) at the B3LYP level using the basis set 6-31G(d) or 6-311G(d,p) as implemented in

Gaussian 03.[34] The calculated frequency was scaled by 0.9613 and 0.9669 for the 6-31G(d) and 6-311G(d,p) basis sets, respectively.[35] The polarizable continuum model (PCM) and cluster model were used to include the solvent effects. The PCM approach includes the solvent effects in such a way that solvent is treated as a dielectric continuum and a solute is subjected to the solvent reaction field in a cavity.[36,37] To examine the structural change of pNA due to the dielectric response of solvents, PCM calculations were performed for model solvents of cyclohexane (dielectric constant $\epsilon = 2.02$), benzene ($\epsilon = 2.25$), tetrahydrofuran ($\epsilon = 7.58$), methanol ($\epsilon = 32.6$), acetonitrile ($\epsilon = 36.6$), and ambient water ($\epsilon = 78.4$). In a cluster model approach, pNA−water clusters in which a few water molecules are attached to the $NO_2$ and/or $NH_2$ groups were used to include the effect of intermolecular hydrogen bonding. To assess the contribution of the local vibrational motion to the normal mode, the potential energy distribution (PED) was calculated from the Gaussian 03 output using the vibrational analysis program MOLVIB.[38] To predict the electronic absorption spectra, the time-dependent DFT method with B3LYP combination was used with the same basis set used for ground-state calculations. All DFT computations were carried out by a Fujitsu Primepower HPC2500 at the Academic Center for Computing and Media Studies, Kyoto University.

## 3. Results

**3.1. $NO_2$ Stretching Mode.** As described in the Introduction, pNA is known to have two $NO_2$ stretching modes (1300−1330 $cm^{-1}$).[26–30] Figure 1a−c shows the resonance Raman spectra (800−1400 $cm^{-1}$) of pNA measured under various pressures and temperatures of (a) water, (b) methanol, and (c) ethanol. The $NO_2$ stretching modes show a remarkable change for all the solvents as a function of pressure and temperature. There are two main characteristics to the spectral changes: (1) the lower-frequency band in the $NO_2$ stretching region gradually loses intensity with increasing temperature (or decreasing density), and the higher-frequency band becomes dominant under supercritical conditions; (2) the higher-frequency band shifts to higher frequencies with decreasing pressure (or decreasing density) under supercritical conditions.

It is interesting how this change in the vibrational mode correlates with the solvatochromic shift of pNA in SCW and scAlcohols. Figure 2 shows a plot of the band peak frequency of the higher-frequency $NO_2$ stretching mode ($\nu_{NO2}$) against the absorption band peak energy of the $S_1 \leftarrow S_0$ transition of pNA. The absorption band peak energy was determined by fitting the spectrum to a log-normal function. The vibrational frequency $\nu_{NO2}$ was determined by fitting the bands around the $NO_2$ stretching region to two Gaussian functions. When the higher-frequency band was dominant, the value of $\nu_{NO2}$ was determined by fitting only the higher-frequency side of the band to a Gaussian function. In water, from 373 to 623 K along the 30.4 MPa isobar, $\nu_{NO2}$ could not be determined unambiguously because the two $NO_2$ stretching bands overlapped considerably. As is shown in Figure 2, $\nu_{NO2}$ has a V-shaped correlation with the absorption band peak energy; i.e., on the red side, $\nu_{NO2}$ decreases with increasing absorption band peak energy, while the tendency becomes opposite on the blue side (>27 500 $cm^{-1}$). In Figure 2, the results for SCW and scAlcohols cover the region spanned by nonpolar solvents such as benzene, carbon tetrachloride, and cyclohexane. In this sense, the $NO_2$ stretching motion is not strongly affected by the hydrogen-bonding character of water and alcohol molecules, and the solvent effects of SCW and scAlcohols appear to be similar to those of nonpolar solvents, from the viewpoint of the absorption band peak (stabilization of the excited-state by solvents) and the $NO_2$ stretching mode (charge separation in the ground-state induced by solvent). However, this is not true, at least for the $NH_2$ stretching mode that is presented in section 3.2.

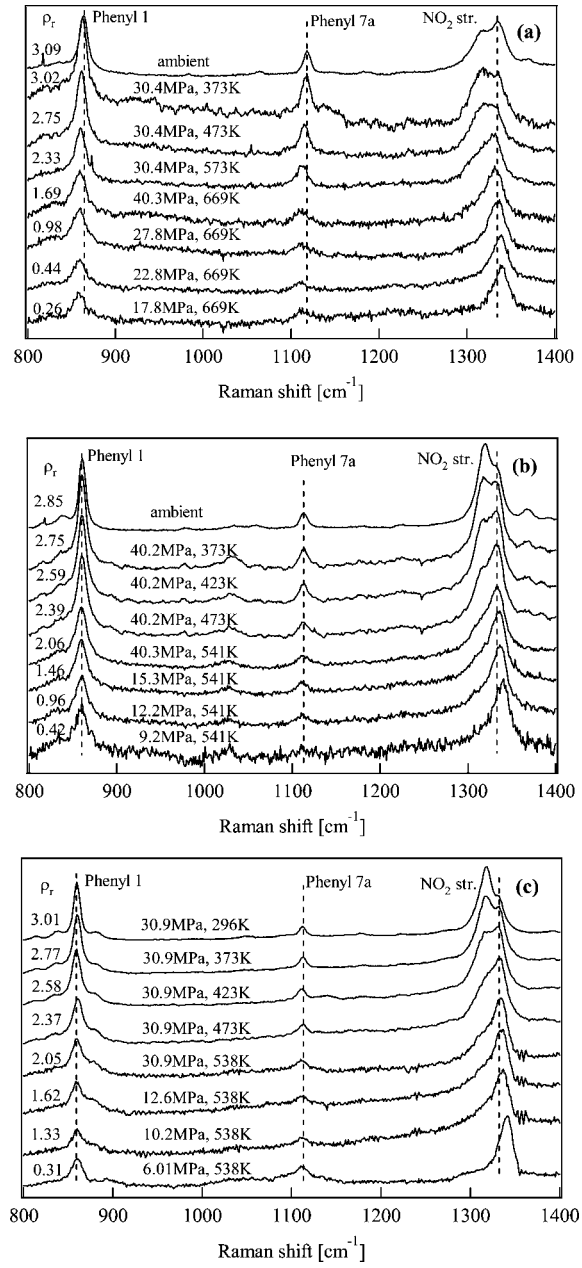


**Figure 1.** Resonance Raman spectra of pNA (800−1400 $cm^{-1}$ region) at different temperatures and pressures in (a) water, (b) methanol, and (c) ethanol. The excitation wavelength is 355 nm for water and methanol solution, and 363.8 nm for ethanol solution.

**3.2. $NH_2$ Stretching Mode.** There were difficulties in taking the measurements of the $NH_2$ stretching mode under high pressures and high temperatures because the Raman band for the $NH_2$ stretching mode of pNA overlapped significantly with the strong Raman signal from the OH stretching mode of the solvent and the fluorescent background from the sapphire window of the high-pressure cell. The $NH_2$ stretching mode was not observed under resonance conditions, as it is not coupled to the conjugated system,[39] and the nonresonance Raman spectrum of the $NH_2$ stretching mode was not detected in aqueous solution because of the low solubility of pNA in water (~1 mM). Therefore, the nonresonance Raman spectra were

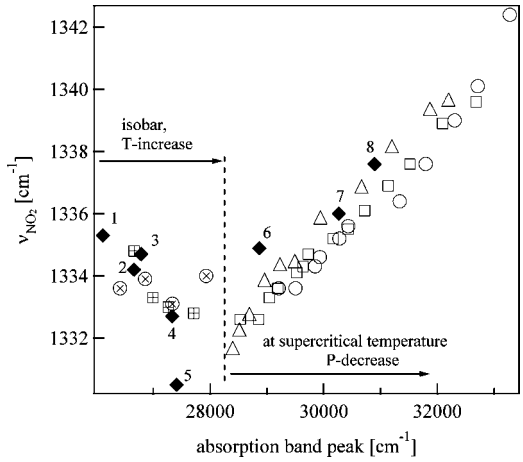


**Figure 2.** Correlation between the frequency of the $NO_2$ stretching mode ($\nu_{NO2}$) and the absorption band peak. ♦: (1) water, (2) methanol, (3) ethanol, (4) acetonitrile (5) tetrahydrofuran, (6) benzene, (7) carbon tetrachloride, (8) cyclohexane; ⊗: in ethanol from room temperature to 473 K at 30.9 MPa; ⊞: in methanol from room temperarture to 473 K at 40.2 MPa; Δ: in SCW (669 K); □: in supercritical methanol (scMeOH; 541 K); ○: in scEtOH (538 K).

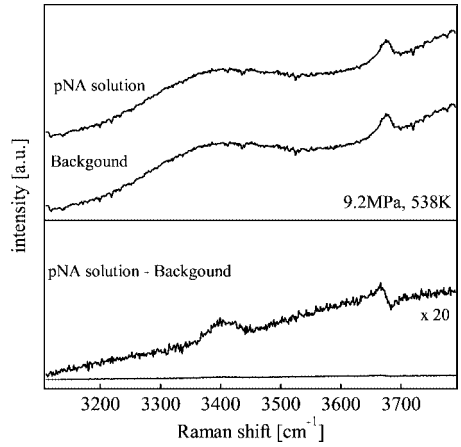


**Figure 3.** Upper panel: Raman spectra for the $NH_2$ stretching region of pNA in methanol at 538 K and 9.2 MPa for the pNA solution and for pure methanol taken under the same experimental geometry. Lower panel: Extracted spectra from the subtraction of the background.

only measured in highly concentrated alcohol solutions (~50 mM). Figure 3 shows Raman signals for a pNA solution of methanol and pure methanol successively measured under the same experimental conditions (9.2 MPa and 538 K). Although the Raman band of the $NH_2$ stretching mode was extremely weak in comparison with the background signals from the solvent and the high-pressure windows, the Raman spectrum of the $NH_2$ stretching region was extracted by subtraction of the background. The residual background (the slope in Figure 3b) was subtracted from the signal by fitting the background region of the spectrum to a smooth function (polynomial function of wavenumber).

Figure 4 shows the nonresonance Raman spectra around the $NH_2$ symmetric stretching region of pNA at various pressures and temperatures for (a) methanol and (b) ethanol. Splitting of the $NH_2$ stretching mode was observed in alcohols. One possible reason for the splitting is the existence of two distinct $NH_2$ groups with and without hydrogen bonding to the solvent. However, the $ND_2$ stretching mode of isotopically substituted pNA did not show such splitting, as shown in Figure 5. The splitting of the $NH_2$ (or NH) stretching mode has been reported in hydrogen-bonded complexes such as thioacetamide−ethanol

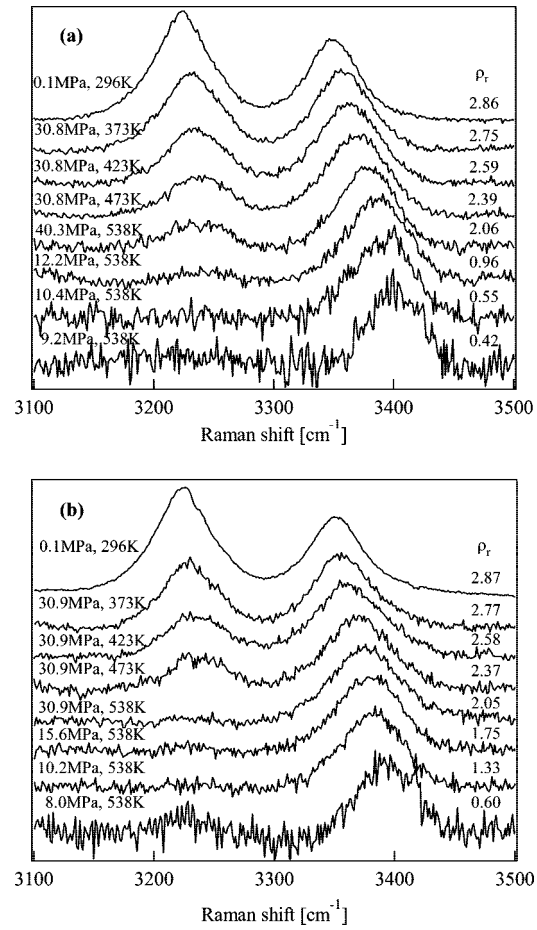


**Figure 4.** Raman spectra (514.5 nm probe) of the $NH_2$ stretching region at different temperatures and pressures in (a) methanol and (b) ethanol.

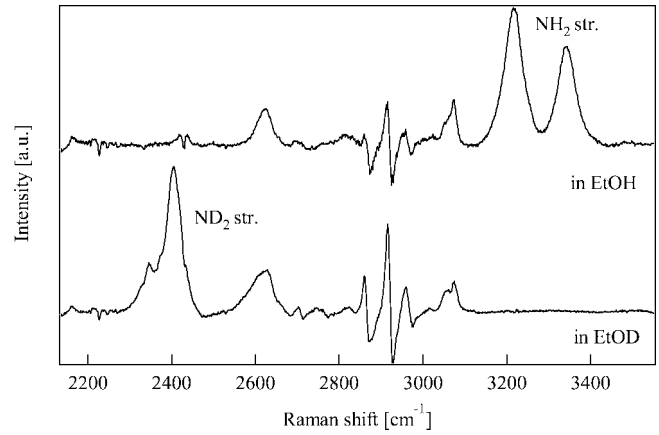


**Figure 5.** Raman spectra of the $NH_2$ stretching mode of pNA and the $ND_2$ stretching mode of pNA-$d_2$. Upper spectra: $NH_2$ stretching mode of pNA in ethanol. Lower spectra: $ND_2$ stretching mode of deuterated pNA-$d_2$ in $C_2H_5OD$.

complex and 7-azaindole dimer.[40,41] In these reports, the most plausible origin of the splitting has been ascribed to Fermi resonance caused by the anharmonic coupling with an overtone or a combination tone involving the $NH_2$ (or NH) bending mode. Therefore, a similar mechanism is considered to underlie the splitting of the $NH_2$ stretching mode for pNA.

As is shown in Figure 4, the $NH_2$ stretching mode had a large frequency shift (~50 cm$^{-1}$) with decreasing density. At the same time, the lower-frequency band reduced intensity and the splitting disappeared. We conclude that this disappearance is

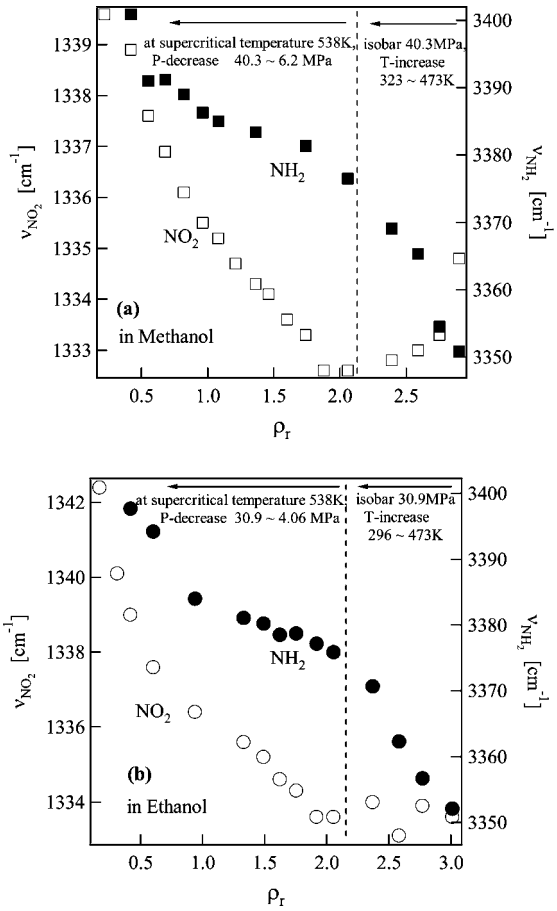


**Figure 6.** Density dependence of the frequencies of $NO_2$ and $NH_2$ stretching modes in (a) methanol and (b) ethanol. Closed and open symbols represent $NO_2$ and $NH_2$ stretching modes, respectively.

because of the increasing frequency gap with temperature between the $NH_2$ stretching mode and the forbidden transition that gains intensity from Fermi resonance.

In Figure 6, the peak frequency of the $NH_2$ stretching mode ($\nu_{NH2}$) is plotted against the reduced density ($\rho_r = \rho/\rho_c$; $\rho_c$: critical density) together with $\nu_{NO2}$. Here we used the peak of the higher-frequency band when the $NH_2$ stretching mode was split. The peak frequency was determined by fitting the band to a Gaussian function. It is apparent that the density dependence of $\nu_{NH2}$ is quite different from that of $\nu_{NO2}$, especially in the high-density region around a $\rho_r$ of 2−3 (isobaric, temperature up to 473 K). The $NH_2$ stretching mode shows a large frequency shift (~25 $cm^{-1}$) with the temperature rising to 473 K. On the other hand, $\nu_{NO2}$ shows only a small frequency shift for alcohols. In the medium- to low-density regions below $\rho_r = 2$, the density dependence of $\nu_{NO2}$ and $\nu_{NH2}$ is rather similar. Both $\nu_{NO2}$ and $\nu_{NH2}$ show a large frequency shift in the low-density region after the moderate shift in the medium density region. This is typical for the effect of the local density enhancement, which has been observed in many supercritical fluids.[19,20] However, it also should be noted that the shift of $\nu_{NH2}$ is more moderate than that of $\nu_{NO2}$ in the medium density region ($\rho_r$: 1−2).

The difference between $\nu_{NH2}$ and $\nu_{NO2}$ is more apparent when $\nu_{NH2}$ is plotted against the absorption peak energy (Figure 7). Although $\nu_{NH2}$ tends to blue shift with the blue shift of the absorption peak, the correlation is not as good as that for $\nu_{NO2}$. For solvents with hydrogen-bonding ability such as scAlcohols, the frequency is somewhat smaller than that for nonpolar solvents such as benzene and carbon tetrachloride with similar

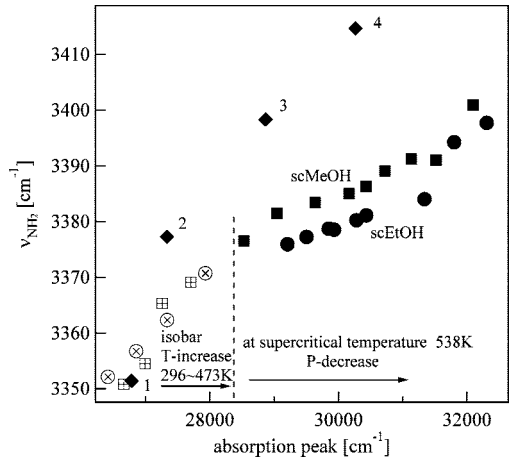


**Figure 7.** Correlation between the frequency of the $NH_2$ stretching mode ($\nu_{NH2}$) and the absorption band peak. ♦: (1) methanol, (2) acetonitrile, (3) benzene, (4) carbon tetrachloride; ⊗: in ethanol from room temperature to 473 K at 30.9 MPa; ⊞: in methanol from room temperature to 473 K at 40.2 MPa; ■: in scMeOH (541 K); ●: in scEtOH (538K).

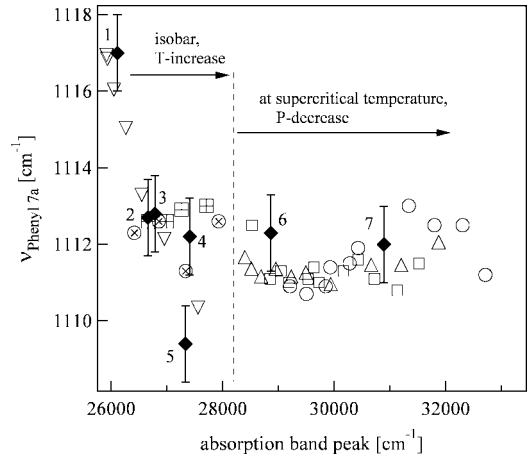


**Figure 8.** Correlation between the frequency of the benzene ring skeletal vibrational mode phenyl-7a ($\nu_{phenyl\text{-}7a}$) and the absorption band peak. ♦: (1) water, (2) methanol, (3) ethanol, (4) acetonitrile (5) tetrahydrofuran, (6) benzene, (7) cyclohexane; ⊗: in ethanol from room temperature to 473 K at 30.9 MPa; ⊞: in methanol from room temperature to 473 K at 40.2 MPa; ▽: in water from room temperature to 623 K at 30.4 MPa; □: in scMeOH (541 K); ○: in scEtOH (538 K); Δ: in SCW (669 K).

absorption peak positions. This frequency difference clearly indicates hydrogen bonding between the $NH_2$ group and alcohol molecules in the supercritical phase.

**3.3. Benzene Ring Skeletal Vibrational Mode.** Before detailed discussion on the solvent density effect on $\nu_{NO2}$ and $\nu_{NH2}$, we briefly mention the density dependence of benzene ring skeletal vibrational modes, such as phenyl-1 (~860 $cm^{-1}$) and phenyl-7a (~1111 $cm^{-1}$). These modes shifted to lower frequencies with increasing temperature only in water (Figure 1a), while they did not show any pressure dependence under supercritical conditions at 669 K. The frequencies of phenyl-1 and phenyl-7a shifted by about 3 and 6 $cm^{-1}$, respectively, with the temperature increasing to 669 K.

Figure 8 shows the frequency of the benzene ring skeletal vibrational mode phenyl-7a ($\nu_{phenyl\text{-}7a}$; determined by the fit to a Gaussian function) against the absorption peak energy. $\nu_{phenyl\text{-}7a}$ is almost independent of the absorption band peak energy except in the region 26000−27000 $cm^{-1}$, which corresponds to the isobaric temperature change of water from room

**TABLE 1: Structural Information on pNA Obtained by Geometry Optimization Using the PCM Model at the B3LYP/6-311G(d,p) Level**

| solvent | $\varepsilon^a$ | $\mu$/D$^b$ | $\theta$/° $^c$ | $L$(C−NH$_2$)/Å$^d$ | $L$(N−O)/Å$^d$ | $L$(N−H)/Å$^d$ | $\nu_{S0\rightarrow S1}$/cm$^{-1}$ $^e$ |
|---|---|---|---|---|---|---|---|
| gas | 1.00 | 7.19 | 19.3 | 1.37689 | 1.22735 | 1.00739 | 32834 |
| cyclohexane | 2.02 | 7.41 | 17.4 | 1.37064 | 1.23006 | 1.00752 | 30731 |
| benzene | 2.25 | 7.43 | 17.4 | 1.37006 | 1.23042 | 1.00758 | 30471 |
| tetrahydrofuran | 7.58 | 7.68 | 14.7 | 1.36261 | 1.23387 | 1.00763 | 29498 |
| methanol | 32.6 | 7.75 | 15.1 | 1.36070 | 1.23548 | 1.00811 | 29244 |
| acetonitrile | 36.6 | 7.83 | 12.6 | 1.35839 | 1.23574 | 1.00758 | 29161 |
| water | 78.4 | 7.87 | 11.9 | 1.35738 | 1.23611 | 1.00760 | 29091 |

$^a$ $\varepsilon$: dielectric constant of solvent. $^b$ $\mu$: dipole moment of pNA. $^c$ $\theta$: out-of-plane angle of the NH$_2$ group. $^d$ $L$(C−NH$_2$), $L$(N−O), $L$(N−H): bond lengths of the C−NH$_2$, N−O, and N−H bonds, respectively, where $L$(N−O) and $L$(N−H) are the averaged bond lengths of the two N−O and N−H bonds, respectively. $^e$ $S_1 \leftarrow S_0$ transition energy obtained by time-dependent DFT calculation.

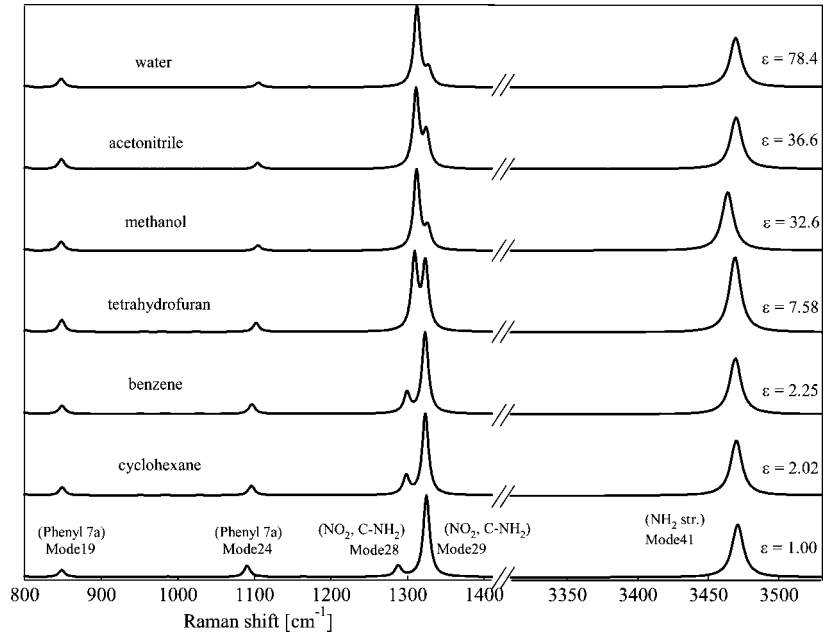


**Figure 9.** Calculated Raman spectra of pNA using the PCM model (B3LYP/6-311G(d,p) level). The mode number and contributing vibrational motion are shown.

temperature to 623 K. A similar correlation was also found for phenyl-1 (see Supporting Information). At high temperatures, the vibrational excited-state of low-frequency modes might contribute to the lower-frequency shift due to the anharmonic coupling with the benzene ring skeletal vibrational modes.[42] However, the benzene ring skeletal vibrational modes did not shift for alcohols up to 538 K (Figure 1b,c). Therefore, the temperature dependence of the benzene ring modes observed in aqueous solution originates from other effects. We conclude that the temperature dependence is induced by the structural change of the benzene ring due to the variation of the charge separation for pNA by surrounding water molecules, as in the case of the $NO_2$ stretching mode, which is discussed in detail in the following section.

## 4. Discussion

**4.1. Computational Approach.** To understand the effect of the solvent on the solute structure and on the Raman spectrum, we first compare the experimental results with the PCM calculations for the electronic states of pNA obtained via B3LYP/6-311G(d,p) level optimization. Table 1 summarizes the structural information of the optimized structures for different model solvents. An apparent change was found in the out-of-plane angle of the $NH_2$ group ($\theta$), which decreases with an increase in the dielectric constant of the solvent. This change is caused by the charge separation of pNA. As is shown in Table 1, the dipole moment ($\mu$) of pNA increases with an increase in the dielectric constant. Since the $NH_2$ group in the charge-separated state has an $sp^2$ character (Scheme 1B), the increase in the dipole moment accompanies the decrease in $\theta$. The charge separation also affects the N−O and C−NH$_2$ bond lengths. As is expected from Scheme 1, the N−O bond length increases with increasing charge separation, while the C−NH$_2$ bond length decreases. The variation in the C−NH$_2$ bond length is twice that for the N−O bond. The N−H bond length is almost unchanged by PCM calculations. The $S_1 \leftarrow S_0$ transition energy ($\nu_{S1\leftarrow S0}$) calculated by the time-dependent DFT method monotonically decreases with increasing solvent dielectric constant.

Figure 9 shows the calculated Raman spectra. The striking feature is that the two normal modes (modes 28 and 29) that have $NO_2$ symmetric stretching vibration show remarkable changes in intensities with solvent. The local vibrations that mainly contribute to modes 28 and 29 are the $NO_2$ stretching vibration, the C−NH$_2$ stretching vibration, and the benzene ring deformation. In modes 28 and 29, the $NO_2$ group and C−NH$_2$ bond vibrate with opposite phases and vibrate in phase, respectively. In the gaseous phase ($\epsilon = 1.00$), mode 29 is dominant over mode 28. However, the intensity of mode 29 decreases with an increase in $\epsilon$, while the intensity of mode 28 increases. Around tetrahydrofuran ($\epsilon = 7.58$), the mode intensities are comparable, and mode 28 becomes dominant for model water ($\varepsilon = 78.4$). This feature qualitatively captures the observed

**TABLE 2: Vibrational Frequencies and PEDs of Modes 28 and 29 Calculated by the PCM Model**

| solvent | $\varepsilon^a$ | $\nu^b$(cm$^{-1}$) | $I^c$ | PED($NO_2$) (%) | PED(C−$NH_2$) (%) | PED(ring deform) (%) |
|---|---|---|---|---|---|---|
| | | | Mode 28 | | | |
| gas | 1.00 | 1287.8 | 57.7 | 4 | 47 | 42 |
| cyclohexane | 2.02 | 1298.2 | 96.2 | 8 | 43 | 41 |
| benzene | 2.25 | 1299.2 | 103.5 | 8 | 44 | 39 |
| tetrahydrofuran | 7.58 | 1309.1 | 288.5 | 28 | 28 | 24 |
| methanol | 32.6 | 1311.1 | 387.9 | 39 | 19 | 19 |
| acetonitrile | 36.6 | 1311.8 | 443.8 | 45 | 14 | 13 |
| water | 78.4 | 1312.3 | 466.8 | 49 | 12 | 12 |
| | | | Mode 29 | | | |
| gas | 1.00 | 1324.7 | 440.7 | 71 | 3 | 4 |
| cyclohexane | 2.02 | 1323.2 | 425.7 | 65 | 6 | 8 |
| benzene | 2.25 | 1323.0 | 420.9 | 64 | 6 | 8 |
| tetrahydrofuran | 7.58 | 1323.3 | 259.9 | 39 | 20 | 25 |
| methanol | 32.6 | 1324.6 | 165.4 | 26 | 28 | 34 |
| acetonitrile | 36.6 | 1326.4 | 111.6 | 19 | 32 | 38 |
| water | 78.4 | 1327.5 | 90.5 | 16 | 35 | 40 |

[a] $\varepsilon$: solvent dielectric constant. [b] $\nu$: calculated vibrational frequency with a scaling factor of 0.9669. [c] $I$: calculated Raman activity.

temperature dependence of the $NO_2$ stretching modes in SCW and scAlcohols in the present study as well as the solvent polarity dependence reported previously,[26–30] i.e., the intensity of the higher frequency band decreases with increasing temperature (or decreasing solvent polarity) in SCW and scAlcohols.[43,44] There has been some debate on the reason for the two $NO_2$ stretching modes in pNA. Two explanations have been suggested as plausible reasons: one supports Fermi resonance, and the other supports the existence of two different solvated forms of pNA.[29,30] However, our calculations indicate there are two characteristic $NO_2$ stretching modes from 42 normal modes in pNA. In this paper, we interpret the observed solvent effect in SCW and scAlcohols as the competition of these two normal modes within the framework of the harmonic approximation.

The PEDs of modes 28 and 29 are summarized in Table 2. What is interesting is that the distribution of these PEDs is significantly dependent on the dielectric constant of the solvent. In a gaseous phase ($\epsilon = 1.00$), the C−$NH_2$ stretching vibration and the benzene ring deformation mainly contribute to mode 28, while the $NO_2$ stretching vibration mainly contributes to mode 29. With an increase in the solvent dielectric constant, the PEDs of the C−$NH_2$ stretching vibration and the benzene ring deformation in mode 28 decrease, and the PED of the $NO_2$ stretching vibration gradually increases. The opposite trend is found for mode 29: the PED of the $NO_2$ stretching vibration decreases, and the PEDs of the C−$NH_2$ stretching vibration and the benzene ring deformation increase with an increase in the solvent dielectric constant. As a result, the distribution of PEDs switches between the conditions of gas and water. It is to be noted that Raman activity ($I$ in Table 2) generally increases with the PED of the $NO_2$ stretching vibration. Specifically, modes 28 and 29 gain intensity mostly from the $NO_2$ stretching vibration. Therefore, the changing of the Raman intensities of the two modes is attributed to the changing of the PED of the $NO_2$ stretching vibration due to the charge separation of pNA.

Although PCM calculations give useful information on the behavior of the intensities of the $NO_2$ stretching modes, the calculated frequency shift for mode 29 poorly reproduces the observed V-shape dependence of the $NO_2$ stretching mode on absorption peak energy. According to the calculation results in Table 2, the vibrational frequency of mode 29 has a somewhat nonmonotonic shift with increasing solvent dielectric constant. However, it mostly has a higher-frequency shift with increasing solvent dielectric constant (or decreasing absorption peak energy) contrary to the experimental observation, where lower-frequency shift mostly occurred with decreasing absorption peak energy (Figure 2). We conclude that this is partially because the decrease in the N−O bond length is somewhat smaller than the increase in the C−$NH_2$ bond length (Table 1) and partially because the structural change of pNA is estimated to be small within the PCM model where the solvent is replaced by the dielectric continuum. Therefore, we also performed the calculation for pNA−water clusters with intermolecular hydrogen bonding directly included. In the calculation for a cluster with one water molecule, a water molecule was first placed in a position around the $NO_2$ or $NH_2$ groups. Geometrical optimization was then performed. In the case of a cluster with two water molecules, three cases were tested: both water molecules on the $NO_2$ side, both on the $NH_2$ side, and one on the $NO_2$ side and the other on the $NH_2$ side. For both molecules being on the $NH_2$ side, we could not obtain any converged solution, or, if there was convergence, the cluster was energetically unfavorable. In the case of a cluster with three water molecules, only one initial configuration was tested: two molecules on the $NO_2$ side and one on the $NH_2$ side.

**SCHEME 2: Model Cluster Optimized by the DFT Calculation**

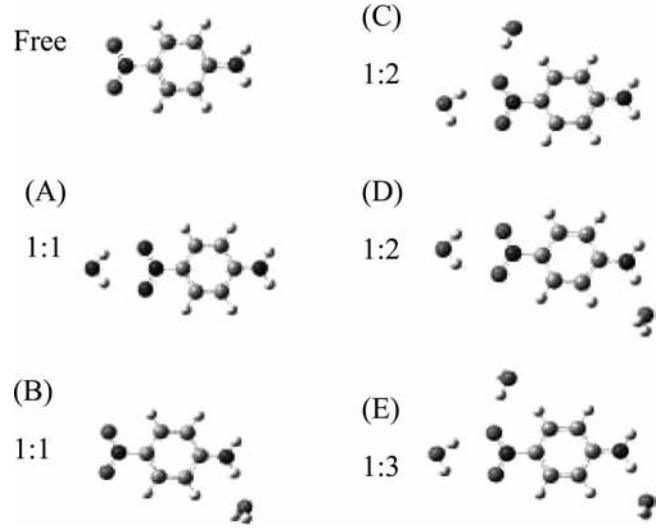


Scheme 2 shows a schematic illustration of the optimized clusters and Table 3 shows the structural information of the energy-minimized pNA−water clusters given by DFT calculations (B3LYP/6-31G(d)).[45] The out-of-plane angle $\theta$ of the $NH_2$

**TABLE 3: Structural Information Obtained by the Geometry Optimization of pNA−Water Clusters at the B3LYP/6-31G(d) Level**

| pNA−$H_2O$ cluster[a] | $\Delta E$/kcal mol$^{-1}$[b] | $\theta$/° [c] | $L$(C−$NH_2$)/Å[d] | $L$(N−O)/Å[e] | $L$(N−H)/Å[d] | $\nu_{S0\rightarrow S1}$/cm$^{-1}$ [e] |
|---|---|---|---|---|---|---|
| free | 0 | 20.8 | 1.38045 | 1.23442 | 1.01067 | 33037 |
| (A) 1:1 | −32.6 | 18.5 | 1.37457 | 1.23770 | 1.01013 | 31787 |
| (B) 1:1 | −35.3 | 15.1 | 1.36774 | 1.23604 | 1.01344 | 32067 |
| (C) 1:2 | −66.2 | 16.8 | 1.37140 | 1.24039 | 1.00978 | 30882 |
| (D) 1:2 | −70.2 | 10.0 | 1.36092 | 1.23986 | 1.01299 | 30949 |
| (E) 1:3 | −100.9 | 7.3 | 1.35795 | 1.24291 | 1.01292 | 30213 |

[a] See Scheme 2. [b] $\Delta E$: stabilization energy from the attachment of water molecules defined by $\Delta E = E$(cluster) − $E$(free pNA) − $E$(free water). [c] $\theta$: out-of-plane angle of the $NH_2$ group. [d] $L$(C−$NH_2$), $L$(N−O), $L$(N−H): bond lengths of the C−$NH_2$, N−O, and N−H bonds, respectively, where $L$(N−O) and $L$(N−H) are the averaged bond lengths of the two N−O and N−H bonds, respectively. [e] $S_1 \leftarrow S_0$ transition energy obtained by the time-dependent DFT calculation.

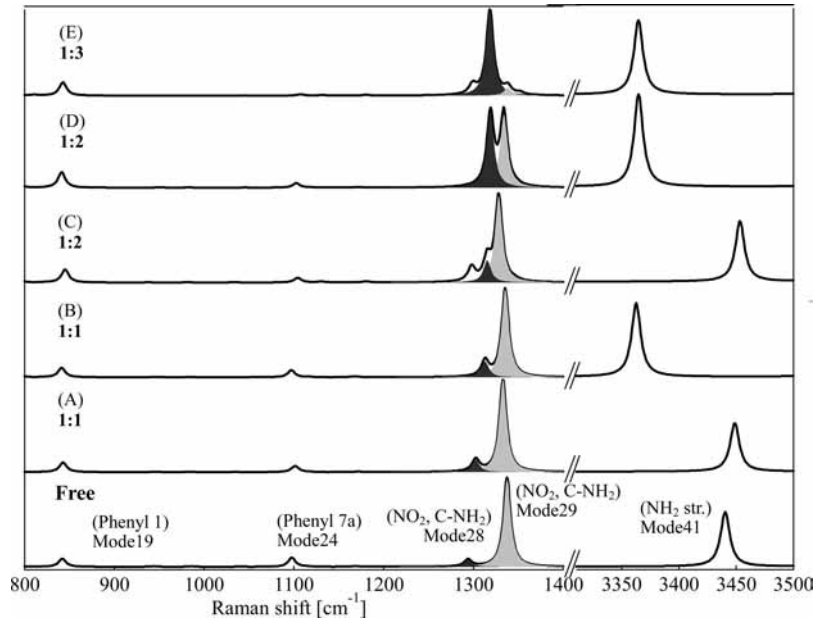


**Figure 10.** Calculated Raman spectra of pNA−water clusters (B3LYP/6−31G(d) level). The contributions of modes 28 and 29 are illustrated.

group also changes as in the case of the PCM calculation. The angle decreases in accordance with the charge separation with increasing cluster size. In fact, the absolute values of Mulliken charge for the nitrogen (+) atom and oxygen (−) atom of the $NO_2$ group, and the carbon (+) atom and nitrogen (−) atom of C−$NH_2$ group increase with the attachment of water molecules. The N−O and the C−$NH_2$ bond lengths also change in accordance with the induced charge separation in the clusters. The charge separation weakens (strengthens) the N−O bond (C−$NH_2$ bond), although changes in the bond lengths are larger than those in PCM calculations for the case of water ($\epsilon = 78.4$). The calculated Raman spectra of the clusters are shown in Figure 10. A remarkable dependence of the intensities of the $NO_2$ stretching modes is found, as in the case of the PCM calculation. The intensities switch between that for free pNA and that for 1:3 (pNA−water) clusters. The PEDs of each mode are given in Table 4. The mechanism of the intensity switching is explained in the same manner as for PCM calculations. If we assume the variation in cluster size corresponds to the change in solvent density going from the gaseous to the liquid state of water, the cluster model also reproduces the frequency shift of the $NO_2$ stretching modes qualitatively, although such clusters only capture a small fraction of the configurations and interactions present in the solution. Mode 29 first shifts to lower frequencies, and then to higher frequencies with increasing cluster size (or decreasing absorption peak), which coincides with the observed trend in Figure 2. We found that the direction of the frequency shift appears to be determined by the PED distribution. Modes 28 and 29 have a tendency to shift to lower frequencies with an increase in the charge separation (or cluster size) when the PED of the $NO_2$ stretching vibration is dominant. On the other hand, these modes have a tendency to shift to higher frequencies with an increase in the charge separation when the PEDs of the C−$NH_2$ stretching vibration and benzene ring deformation are dominant. This is because the charge

**TABLE 4: Vibrational Frequencies and PEDs of Modes 28 and 29 Calculated from the Cluster Model**

| cluster[a] pNA:$H_2O$ | $\nu^b$ (cm$^{-1}$) | $I^c$ | PED($NO_2$) (%) | PED(C−$NH_2$) (%) | PED(ring deform) (%) |
|---|---|---|---|---|---|
| | | | Mode 28 | | |
| free | 1294.0 | 34.9 | 1 | 50 | 43 |
| (A) 1:1 | 1302.5 | 77.6 | 5 | 46 | 42 |
| (B) 1:1 | 1312.9 | 82.5 | 7 | 43 | 41 |
| (C) 1:2 | 1315.2 | 119.1 | 11 | 23 | 56 |
| (D) 1:2 | 1318.8 | 351.2 | 29 | 25 | 24 |
| (E) 1:3 | 1318.2 | 550.1 | 52 | 2 | 18 |
| | | | Mode 29 | | |
| free | 1337.4 | 443.3 | 71 | 1 | 3 |
| (A) 1:1 | 1332.8 | 583.9 | 64 | 3 | 6 |
| (B) 1:1 | 1335.3 | 462.9 | 63 | 5 | 9 |
| (C) 1:2 | 1328.0 | 466.5 | 52 | 12 | 18 |
| (D) 1:2 | 1333.8 | 354.2 | 36 | 20 | 28 |
| (E) 1:3 | 1338.2 | 50.2 | 6 | 33 | 48 |

[a] See Scheme 2. [b] $\nu$: calculated vibrational frequency with a scaling factor of 0.9613. [c] $I$: calculated Raman activity.

separation weakens the N−O bond, while it strengthens the C−$NH_2$ bond (Tables 1 and 3).

The calculated benzene ring skeletal vibrational modes (phenyl-7a and phenyl-1) slightly shift to higher frequencies with the attachment of a water molecule to the $NO_2$ or $NH_2$ groups. This trend coincides with the density effect of water in the higher-density region ($\rho_r > 2$) and supports the frequency shift being attributed to the structural change from the charge separation induced by the surrounding water molecules.

The $NH_2$ stretching mode shows a large lower-frequency shift ($\sim$80 $cm^{-1}$) with the attachment of a water molecule, reflecting the effect of the specific intermolecular interaction, which is absent in the PCM approach. In contrast to the case of the $NO_2$ stretching mode, the splitting of the $NH_2$ stretching mode was not obtained by a calculation at the harmonic level. This also supports the consideration that anharmonic coupling, such as Fermi resonance, plays an important role in splitting the $NH_2$ stretching mode. Experimentally, the apparent frequency shift of the $NH_2$ stretching mode from an ambient condition to the supercritical temperature at the lowest density ($\rho_r = 0.42$) is about 50 $cm^{-1}$ in the case of methanol. The calculated frequency shift ($\sim$80 $cm^{-1}$) seems to be too large (we also checked that the attachment of a methanol molecule to the $NH_2$ group caused a 74 $cm^{-1}$ shift of the $NH_2$ stretching mode).[46] In the following section, we present a more detailed discussion on the extent of hydrogen-bonding.

Although the $NO_2$ stretching mode was discussed for our DFT calculations at the harmonic level, we do not deny the possibility that the splitting mechanism due to anharmonic coupling, such as Fermi resonance, is part of the mechanism for the splitting of the $NO_2$ stretching mode as discussed above.[30] If there is a strong anharmonic coupling involving the $NO_2$ stretching modes, the frequencies and intensities of the $NO_2$ stretching modes are significantly affected. However, it is quite difficult to know the degree of anharmonic coupling. Because the apparent splitting is not observed under supercritical conditions in our experiment, such complexity of the splitting mechanism does not have a direct effect on the main discussion.

**4.2. Hydrogen-Bonding between Solute and Solvent.** Figure 7 clearly indicates the presence of hydrogen-bonding between pNA and solvent, even under supercritical conditions, which seems to contradict the previous estimation of $\beta$ (hydrogen bond basicity) from solvatochromic measurements.[15] The $\beta$ value is determined from a comparison of the absorption peak energies for pNA and *N*,*N*-diethyl-*p*-nitroaniline. As described in section 1, Lu et al. measured several solvatochromic parameters, including $\alpha$ and $\beta$ for scEtOH.[15] They found that $\beta$ is almost equal to zero in the supercritical phase. Oka et al. found that the $\beta$ value is also equal to zero in SCW.[23] However, our results clearly indicate the existence of hydrogen bonding around the $NH_2$ group of pNA in the supercritical phase. Therefore, we point out that $\beta$ is not appropriate for the estimation of hydrogen-bonding in SCW and scAlcohols.

Figure 11 compares the peak shift of $\nu_{NH2}$ with the extent of solvent hydrogen-bonding, which has been studied extensively from NMR and Raman measurements.[7–9] Hoffmann et al. determined the extent of hydrogen-bonding ($\eta$) in ethanol and methanol relative to that for the ambient condition,[8,47] as was done for SCW by Matubayasi et al.[7] They determined $\eta$ for the alcohols by assuming a linear correlation between the chemical shifts of the OH proton and $\eta$, and normalizing it by the value for the ambient condition. To discuss the extent of the hydrogen-bonding between the solute and solvent, it is important to estimate the vibrational frequency of the $NH_2$ mode without

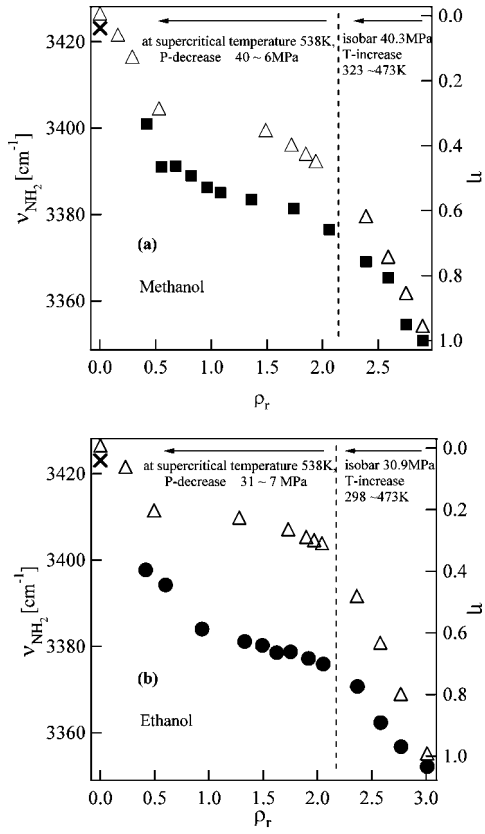


**Figure 11.** Density dependence of the frequencies of $NH_2$ stretching modes ($\nu_{NH2}$) for different degrees of hydrogen bonding ($\eta$) estimated from NMR measurements of neat methanol and ethanol. × indicates the $NH_2$ vibrational frequency of ABN in gas phase as a reference. (a) ■: $\nu_{NH2}$ in methanol; Δ: degree of hydrogen bonding ($\eta$) for methanol. (b) ●: $\nu_{NH2}$ in ethanol; Δ: degree of hydrogen bonding ($\eta$) for ethanol.

solvent. Unfortunately, the value of $\nu_{NH2}$ for pNA in a gaseous phase ($\rho_r = 0$) is not available to the best of our knowledge. Although we tried to measure the Raman spectrum of pNA in the gaseous phase, we found that the vapor of pNA was not stable at high temperature. Instead, the value of $\nu_{NH2}$ for *p*-aminobenzonitrile (ABN) vapor measured at 543 K[48] is shown at $\rho_r \approx 0$ in Figure 11 (3423.1 $cm^{-1}$, shown as an ×). The value of $\nu_{NH2}$ for ABN is expected to be quite similar to that for pNA because (1) the value of $\nu_{NH2}$ for ABN is quite similar to that for pNA in the same liquid solvent (3353 $cm^{-1}$ (ABN) and 3351 $cm^{-1}$ (pNA) in methanol, 3382 $cm^{-1}$ and 3377 $cm^{-1}$ in acetonitrile, 3399 $cm^{-1}$ and 3398 $cm^{-1}$ in benzene, and 3413 $cm^{-1}$ and 3415 $cm^{-1}$ in carbon tetrachloride)[48] and (2) the calculated frequency of the $NH_2$ stretching mode for ABN is similar to that for pNA (3440.4 $cm^{-1}$ (ABN) and 3432.0 $cm^{-1}$ (pNA) for the free molecule (B3LYP/6−31G(d)), and 3362.4 and 3362.5 for a cluster where a water molecule is attached to the $NH_2$ group). Therefore, the frequency of the $NH_2$ stretching mode for ABN vapor is a reasonable estimate for the $\nu_{NH2}$ of pNA in a gaseous phase.

As is shown in Figure 11, the density dependence of $\nu_{NH2}$ has several similarities to that of $\eta$. Both $\nu_{NH2}$ and $\eta$ change significantly with increasing density in the lower-density region ($\rho_r = 0-1$), then have moderate density dependency in the medium-density region ($\rho_r = 1-2$). In the higher density region with decreasing temperature ($\rho_r = 2-3$), $\nu_{NH2}$ and $\eta$ again show remarkable density dependency. This density dependence is interpreted as indicating that hydrogen bonding has been formed in the low-density region ($\rho_r = 0-1$), the number of hydrogen

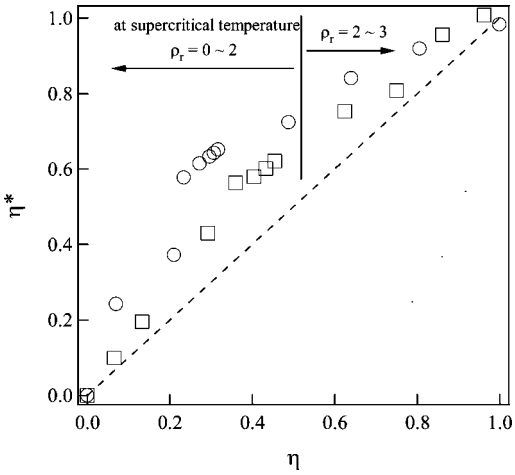


**Figure 12.** Correlation between $\eta$ and $\eta^*$. □: in methanol; ○: in ethanol.

bonds is saturated in the medium-density region ($\rho_r = 1-2$), and that hydrogen-bonding is strengthened with a temperature decrease in the high-density region ($\rho_r = 2-3$). To assess solute−solvent hydrogen bonding, we introduce the strength of hydrogen bonding between solute and solvent ($\eta^*$), by assuming a linear correlation between $\nu_{NH2}$ and $\eta^*$, as

$$\eta^* = \frac{\nu_{NH2} - \nu_{NH2}(\text{gas})}{\nu_{NH2}(\text{ambient}) - \nu_{NH2}(\text{gas})} \quad (1)$$

where $\nu_{NH2}$(gas) is the frequency of the $NH_2$ stretching mode ($\nu_{NH2}$) in the gas phase (3423.1 $cm^{-1}$), and $\nu_{NH2}$(ambient) is $\nu_{NH2}$ in the ambient condition (3351.4 and 3350.9 $cm^{-1}$ in methanol and ethanol, respectively). The correlation between $\eta$ and $\eta^*$ is shown in Figure 12. Although $\eta^*$ changes in parallel with $\eta$, as expected from the similar density dependences for $\nu_{NH2}$ and $\eta$, $\eta^*$ is generally larger than $\eta$ for the same thermodynamic state. Particularly in supercritical phase, $\eta^*$ is 1.5−2 times larger than $\eta$ in the region of $\eta \sim 0.4$. There are two plausible origins for the enhancement of solute−solvent hydrogen-bonding factor. One is the so-called "local" (i.e., hydrogen-bonding site) density enhancement. There are two hydrogen-bond donating sites and one accepting site in the $NH_2$ group. Therefore, the solvent molecules may easily access these hydrogen bonding sites in the medium-density region, which results in larger values of $\eta^*$. The other is the nonlinearity of the vibrational frequency shift due to hydrogen bonding. According to the cluster model calculations, the vibrational frequency shift of the $NH_2$ stretching mode is not a linear function of the number of hydrogen bonds (the details of the calculation results on methanol clusters are given in the Supporting Information, Scheme S1, Tables S1 and S2, and Figure S1).[49] The effect of the second solvating molecule on the vibrational frequency is not as large as that of the first solvating molecule. Although the cluster model may exaggerate the real situation, this kind of effect surely affects the vibrational frequency shift of the $NH_2$ stretching mode. Therefore, the presented value of $\eta^*$ may not reflect the "number" of hydrogen bonds itself. To assess solute−solvent hydrogen bonding more quantitatively, a sophisticated electronic state calculation where the realistic solute−solvent interaction is included, such as RISM-SCF and QM/MM approaches, is necessary.

## 5. Conclusion

We investigated the effects of solvent on the $NO_2$ stretching mode, the $NH_2$ stretching mode, and the benzene ring skeletal vibrational mode of pNA in SCW and scAlcohols. The relative intensities of the two $NO_2$ stretching modes changed remarkably with increasing temperature, and the higher-frequency mode of the two became a dominant band above the critical temperature. In the supercritical phase, the higher-frequency band shifted by $\sim$10 $cm^{-1}$. The observed frequency shift displayed a V-shape correlation with the absorption peak energy. The solvent effects of SCW and scAlcohols were similar to those of nonpolar solvents in assessing the $NO_2$ frequency (charge separation induced by solute−solvent interactions) and the absorption peak (the stabilization of the excited state).

The $NH_2$ stretching mode was used as a direct probe for intermolecular hydrogen bonding. The $NH_2$ stretching mode shifted by $\sim$50 $cm^{-1}$ with decreasing density from $\rho_r = 3$ to 0.5. Another $\sim$20 $cm^{-1}$ shift is expected with decreasing density from $\rho_r = 0.5$ to 0 using the $NH_2$ vibrational frequency for ABN in gas phase as a reference. The general density dependence of the frequency shift was similar to that of the degree of hydrogen bonding ($\eta$) of the solvent estimated from NMR measurements. It was demonstrated that the strength of the solute−solvent hydrogen bonding changes in parallel with the strength of the solvent−solvent hydrogen bonding. Solute−solvent hydrogen bonding exists even in the low-density region in terms of a significant difference between the frequencies of the $NH_2$ stretching mode in nonpolar solvents and low-density alcohols.

The frequency of the benzene ring stretching mode showed temperature dependence only in water. The frequency shifted slightly to lower frequencies with increasing temperature. Since the frequency of the benzene ring skeletal vibrational mode correlates with the absorption peak energy as in the case of the $NO_2$ stretching mode, this frequency shift is considered to be attributed to the structural change due to charge separation induced by the strong hydrogen bonding ability of water. This consideration was also supported by the DFT calculation of pNA−water clusters.

DFT calculations were performed at the harmonic level using the PCM model and cluster model. The calculations gave important insights into the mechanism of the intensity change and frequency shift of the $NO_2$ stretching modes. The calculation revealed that the relative intensity change results from the switching of the PED of $NO_2$ between the two normal modes. The pNA−water clusters also reproduced the V-shape correlation between the absorption peak and the frequency of the $NO_2$ stretching mode. The frequency shift is caused by the structural change of pNA due to the charge separation induced by the solvent, and the direction of the shift is determined by the PED balance between $NO_2$ and C−$NH_2$ stretching vibrations. The effect of the anharmonicity on the vibrational mode was not taken into account in our calculations. A future experimental investigation of the anharmonic coupling involving the $NO_2$ stretching mode is of interest. Two-dimensional vibrational spectroscopy would be a powerful approach.[50]

The solvent fluctuation around the solute is an interesting subject particularly in supercritical fluids.[19,51] However, the solvent fluctuation was not assessed in the present study because the Raman bandwidth of the solute is significantly broadened as temperature rises and is unchanged by the control of the density in supercritical phase (Supporting Information). The worse signal-to-noise ratio at low densities also makes the analysis difficult. The detailed analysis of Raman bandwidth in high-temperature fluids remains an issue for future studies.[52,53]

**Acknowledgment.** This work was partially supported by Grants-in-Aid for Scientific Research from JSPS (Nos. 16350010 and 19350010), and by a fund from the Mitsubishi Foundation.

T.F. was supported with a research fellowship from the Global Center of Excellence, International Center for Integrated Research and Advanced Education in Material Science, Kyoto University, Japan. We thank Mr. Koji Osawa (Kyoto University) for measuring the Raman spectra of ABN and also appreciate Prof. Mark Maroncelli's kind help in the calculation of PEDs and fruitful discussions.

**Supporting Information Available:** Schemes of the optimized pNA−methanol clusters. Tables of the optimized energies, structures, vinrational frequencies, and PEDs of pNA−methanol clusters. Figures of Raman spectra calculated for pNA−methanol clusters, the correlation between the vibrational frequency of experimentally determined Phenyl 1 and the absorption band peak, and the solvent density dependence of the bandwidths of the $NO_2$ stretching mode, $NH_2$ stretching mode, and benzene ring skeletal vibrational modes. This material is available free of charge via the Internet at http://pubs.acs.org.

## References and Notes

(1) Weingärtner, H.; Franck, E. U. *Angew. Chem., Int. Ed.* **2005**, *44*, 2672.

(2) Bermejo, M. D.; Cocero, M. J. *AIChE J.* **2006**, *52*, 3933.

(3) Watanabe, M.; Sato, T.; Inomata, H.; Smith, Jr. R. L.; Arai, K.; Kruse, A.; Dinjus, E. *Chem. Rev.* **2004**, *104*, 5803.

(4) Genta, M.; Iwaya, T.; Sasaki, M.; Goto, M. *Waste Manage.* **2007**, *27*, 1167.

(5) Minami, E.; Saka, S. *J. Wood Sci.* **2003**, *49*, 73.

(6) (a) Yamaguchi, T.; Yoshida, K.; Yamamoto, N.; Hosokawa, S.; Inui, M.; Baron, A. Q. R.; Tsutsui, S. *J. Phys. Chem. Solids* **2005**, *66*, 2246. (b) Yamaguchi, T.; Benmore, C. J.; Soper, A. K. *J. Chem. Phys.* **2000**, *112*, 8976.

(7) (a) Matubayasi, N.; Wakai, C.; Nakahara, M. *J. Chem. Phys.* **1997**, *107*, 9133; **1999**, *110*, 8000. (b) Matubayasi, N.; Nakao, N.; Nakahara, M. *J. Chem. Phys.* **2001**, *114*, 4107.

(8) (a) Hoffmann, M. M.; Conradi, M. S. *J. Am. Chem. Soc.* **1997**, *119*, 3811. (b) Hoffmann, M. M.; Conradi, M. S. *J. Phys. Chem. B.* **1998**, *102*, 263.

(9) (a) Tassaing, T.; Danten, Y.; Besnard, M. *J. Mol. Liq.* **2002**, *101*, 149. (b) Lalanne, P.; Andanson, J. M.; Soetens, J. C.; Tassaing, T.; Danten, Y.; Besnard, M. *J. Phys. Chem. A* **2004**, *108*, 3902.

(10) Ikushima, Y.; Hatakeda, K.; Saito, N.; Arai, K. *J. Chem. Phys.* **1998**, *108*, 5855.

(11) (a) Asahi, N.; Nakahara, M. *Chem. Phys. Lett.* **1998**, *290*, 63. (b) Asahi, N.; Nakahara, M. *J. Chem. Phys.* **1998**, *109*, 1319.

(12) Yamaguchi, T.; Matubayasi, N.; Nakahara, M. *J. Phys. Chem. A,* **2004**, *108*, 3902.

(13) Schwarzer, D.; Lindner, J.; Vo1hringer, P. *J. Phys. Chem. A* **2006**, *110*, 2858.

(14) (a) Bennett, G. E.; Johnston, K. P. *J. Phys. Chem.* **1994**, *98*, 441. (b) Niemeyer, E. D.; Dunbar, R. A.; Bright, F. V. *Appl. Chem.* **1997**, *51*, 1547. (c) Minami, K.; Mizuta, M.; Suzuki, M.; Aizawa, T.; Arai, K. *Phys. Chem. Chem. Phys.* **2006**, *8*, 2257. (d) Kometani, N.; Takemiya, K.; Yonezawa, Y.; Amita, F.; Kajimoto, O. *Chem. Phys. Lett.* **2004**, *394*, 85. (e) Osada, M.; Toyoshima, K.; Mizutani, T.; Minami, K.; Watanabe, M.; Adschiri, T.; Arai, K. *J. Chem. Phys.* **2003**, *118*, 4573. (f) Mikami, K.; Ohashi, T.; Suzuki, M.; Aizawa, T.; Adshjiri, T.; Arai, T. *Anal. Sci.* **2006**, *22*, 1417.

(15) Lu, J.; Boughner, E. C.; Liotta, C. L.; Eckert, C. A. *Fluid Phase Equilib.* **2002**, *198*, 37.

(16) Aizawa, T.; Kanakubo, M.; Hiejima, Y.; Ikushima, Y.; Smith, R. L.,Jr. *J. Phys. Chem. A* **2005**, *109*, 7353.

(17) Xiang, T.; Johnston, K. P. *J. Phys. Chem.* **1994**, *98*, 7915.

(18) Blugarevich, D. S.; Sako, T.; Sugeta, T.; Ohtake, K.; Takebayashi, Y.; Kamizawa, C. *J. Chem. Phys.* **1999**, *111*, 4239.

(19) (a) Kajimoto, O. *Chem. Rev.* **1999**, *99*, 355. (b) Tucker, S. C. *Chem. Rev.* **1999**, *99*, 391.

(20) (a) Lewis, J. E.; Biswas, R.; Robinson, A. G.; Maroncelli, M. *J. Phys. Chem.* **2001**, *105*, 3306. (b) Song, W.; Biswas, R.; Maroncelli, M. *J. Phys. Chem.* **2000**, *104*, 6924.

(21) Reichardt, C. *Chem. Rev.* **1994**, *94*, 2319.

(22) See, e.g., Reichardt, C. *Solvents and Solvents Effects in Organic Chemistry*; VCH: Weinheim, Germany, 1988.

(23) Oka, H.; Kajimoto, O. *Phys. Chem. Chem. Phys.* **2003**, *5*, 2535.

(24) Huyskens, F. L.; Huyskens, P. L.; Persoons, A. P. *J. Chem. Phys.* **1998**, *108*, 8161.

(25) Schmid, E. D.; Moschallski, M.; Peticolas, W. L. *J. Phys. Chem.* **1986**, *90*, 2340.

(26) (a) Mohanalingam, K.; Hamaguchi, H. *Chem. Lett.* **1997**, 537. (b) Mohanalingam, K.; Yokoyama, D.; Kato, C.; Hamaguchi, H. *Bull. Chem. Soc. Jpn.* **1999**, *72*, 389.

(27) Moran, A. M.; Kelley, A. M. *J. Chem. Phys.* **2001**, *115*, 912.

(28) Kozich, V.; Werncke, W.; Dreyer, J.; Brzezinka, K.-W.; Rini, M.; Kummrow, A.; Elsaesser, T. *J. Chem. Phys.* **2002**, *117*, 719.

(29) Shigeto, S.; Hiramatsu, H.; Hamaguchi, H. *J. Phys. Chem. A* **2006**, *110*, 3738.

(30) Dreyer, J.; Kozich, V.; Werncke, W. *J. Chem. Phys.* **2007**, *127*, 234505.

(31) Fujisawa, T.; Terazima, M.; Kimura, Y.; Maroncelli, M., *Chem. Phys. Lett.* **2006**, *430*, 303.

(32) (a) Fujisawa, T.; Maru, E.; Amita, F.; Harada, M.; Uruga, T.; Kimura, Y. In *Water, Steam, and Aqueous Solutions for Electric Power*; Proceedings of the 14th International Conference on the Properties of Water and Steam, Kyoto, Japan, 2004; p 445. (b) Kimura, Y.; Amita, F.; Fujisawa, T. *Rev. High Pressure Sci. Technol.* **2006**, *16*, 87.

(33) (a) de Reuck, K M.; Craven, R. J. B. *Methanol/International Thermodynamic Tables of the Fluid State-12, IUPAC*; Blackwell Scientific Publishing: Oxford, 1993. (b) Vargaftik, N. B. *Handbook of Thermophysical Properties of Gases and Liquids*; Nauka: Moscow, 1972. (c) Marshall, W. L.; Franck, E. U. *J. Phys. Chem. Ref. Data* **1981**, *10*, 295.

(34) Frisch, M. J.; Trucks, G. W.; Schlegel, H. B.; Scuseria, G. E.; Robb, M. A.; Cheeseman, J. R.; Montgomery, J. A., Jr.; Vreven, T.; Kudin, K. N.; Burant, J. C.; Millam, J. M.; Iyengar, S. S.; Tomasi, J.; Barone, V.; Mennucci, B.; Cossi, M.; Scalmani, G.; Rega, N.; Petersson, G. A.; Nakatsuji, H.; Hada, M.; Ehara, M.; Toyota, K.; Fukuda, R.; Hasegawa, J.; Ishida, M.; Nakajima, T.; Honda, Y. ; Kitao, O.; Nakai, H.; Klene, M.; Li, X.; Knox, J. E.; Hratchian, H. P.; Cross, J. B.; Bakken, V.; Adamo, C.; Jaramillo, J.; Gomperts, R.; Stratmann, R. E.; Yazyev, O.; Austin, A. J.; Cammi, R.; Pomelli, C.; Ochterski, J. W.; Ayala, P. Y.; Morokuma, K.; Voth, G. A.; Salvador, P.; Dannenberg, J. J.; Zakrzewski, V. G.; Dapprich, S.; Daniels, A. D.; Strain, M. C.; Farkas, O.; Malick, D. K.; Rabuck, A. D.; Raghavachari, K.; Foresman, J. B.; Ortiz, J. V.; Cui, Q.; Baboul, A. G.; Clifford, S.; Cioslowski, J.; Stefanov, B. B.; Liu, G.; Liashenko, A.; Piskorz, P.; Komaromi, I.; Martin, R. L.; Fox, D. J.; Keith, T.; Al-Laham, M. A.; Peng, C. Y.; Nanayakkara, A.; Challacombe, M.; Gill, P. M. W.; Johnson, B.; Chen, W.; Wong, M. W.; Gonzalez, C.; Pople, J. A. *Gaussian 03*; Gaussian, Inc.: Wallingford, CT, 2004.

(35) Irikura, K. K.; Johnson III, R. D.; Kacker, R. N. *J. Phys. Chem. A* **2005**, *109*, 8430.

(36) Tomasi, J.; Persico, M. *Chem. Rev.* **1994**, *94*, 2027.

(37) A sphere was also placed on the hydrogen atom of the $NH_2$ group in the PCM calculation.

(38) Kuczera, K.; Wiorkiewicz-Kuczera, J. *MOLVIB: A Program for Analysis of Molecular Vibrational Spectra*.

(39) Kozich, V.; Dreyer, J.; Ashihara, S.; Werncke, W.; Elsaesser, T. *J. Chem. Phys.* **2006**, *125*, 074504.

(40) (a) Walter, W.; Vinkler, P. *Spectrochim. Acta* **1977**, *33A*, 205. (b) Vinkler, P.; Walter, W.; Keresztury, G. *Spectrochim. Acta* **1980**, *36A*, 935.

(41) Elsaesser, T.; Huse, N.; Dreyer, J.; Dwyer, J. R.; Heyne, K.; Nibbering, E. T. J. *Chem. Phys.* **2007**, *341*, 175.

(42) Hamaguchi, H.; Iwata, K. *Bull. Chem. Soc. Jpn.* **2002**, *75*, 883.

(43) It is to be noted that the observed temperature dependence of the relative intensity of the $NO_2$ stretching modes in water is a little different from that in alcohols. In water, the lower-frequency band is weaker than the higher-frequency band under ambient conditions. This phenomenon is observed only under a resonance condition. The lower-frequency band in water is dominant under a non-resonant condition, as in the case of alcohols.[44] In resonant conditions, the weaker band on the lower-frequency side appears to increase slightly up to 473 K, and then decreases gradually with increasing temperature. We conclude that the anomaly for the relative intensity change of the $NO_2$ stretching modes up to 473 K may reflect the structural change of the excited state of pNA in water

(44) Fujisawa, T.; Terazima, M.; Kimura, Y. *J. Chem. Phys.* **2006**, *124*, 184503.

(45) We found the calculated intensity of the $NO_2$ stretching mode is dependent on the basis set, although the general trends for different basis sets are not greatly different. When the 6-311G(d,p) basis set was used for the calculation of the clusters, mode 28 was significantly split in some conformations as a result of mixing with another benzene ring deformation. On the other hand, the result using the 6-31G(d) basis set agrees with the observed spectra, although similar splitting occurs to a small extent. We also checked the solvent species dependence on the calculation using pNA−methanol clusters. The results are similar to those for pNA−water clusters (see Supporting Information)

(46) The frequency shift of the $NH_2$ stretching mode with the attachment of a water molecule was strongly dependent on the basis set. When 6-311G(d,p) was used, the shift was $\sim$45 $cm^{-1}$, which was about half the shift for 6-31G(d).

(47) The interpolated value of $\eta$ at 538 K is plotted in Figure 11.

(48) Osawa, K.; Hamamoto, T.; Fujisawa, T.; Terazima, M.; Kimura, Y. Manuscript in preparation.

(49) For example, the frequency shift of the $NH_2$ stretching mode by the attachment of a methanol molecule to one hydrogen atom of the $NH_2$ group is$-74.2$ $cm^{-1}$ at the B3LYP/6-31G(d) level. Further attachment of a methanol molecule to the other hydrogen atom of the $NH_2$ group (i.e., 1:2 cluster) induces only a$-5.7$ $cm^{-1}$ shift (see details in Supporting Information).

(50) Eldler, J.; Hamm, P. *J. Chem. Phys.* **2003**, *119*, 2709.

(51) Nishikawa, K.; Ayusawa, A. A.; Morita, T. *J. Supercrit. Fluids* **2004**, *30*, 249.

(52) Cabaco, M. I.; Besnard, M.; Tassaing, T.; Danten, Y. *J. Mol. Liq.* **2006**, *125*, 100.

(53) Rice, S. F.; Wickham, J. J. *J. Raman Spectrosc.* **2000**, *31*, 619.

JP710530M